Alzheimer's & Dementia 12 (2016) 1273-1287

Featured Article

Kallikrein-8 inhibition attenuates Alzheimer's disease pathology in mice

Arne Herring[a,**], Yvonne Münster[a], Tamer Akkaya[a], Sahar Moghaddam[a], Katharina Deinsberger[a], Jakob Meyer[a], Julia Zahel[a], Eduardo Sanchez-Mendoza[b], Yachao Wang[b], Dirk M. Hermann[b], Thomas Arzberger[c,d], Sarah Teuber-Hanselmann[a], Kathy Keyvani[a,*]

[a]Institute of Neuropathology, University of Duisburg-Essen, Essen, Germany
[b]Department of Neurology, University of Duisburg-Essen, Essen, Germany
[c]Department of Psychiatry and Psychotherapy, Ludwig-Maximilians-University Munich, Munich, Germany
[d]Center for Neuropathology and Prion Research, Ludwig-Maximilians-University Munich, Munich, Germany

Abstract

Introduction: Memory loss and increased anxiety are clinical hallmarks of Alzheimer's disease (AD). Kallikrein-8 is a protease implicated in memory acquisition and anxiety, and its mRNA is known to be up-regulated in AD-affected human hippocampus. Therefore, an involvement of Kallikrein-8 in Alzheimer's pathogenesis is conceivable but remains to be proved.

Methods: We determined the cerebral expression of Kallikrein-8 mRNA and protein during the course of AD in patients and in transgenic mice and tested the impact of Kallikrein-8 inhibition on AD-related pathology in mice and in primary glial cells.

Results: Kallikrein-8 mRNA and protein were up-regulated in both species at incipient stages of AD. Kallikrein-8 inhibition impeded amyloidogenic amyloid-precursor-protein processing, facilitated amyloid β (Aβ) clearance across the blood-brain-barrier, boosted autophagy, reduced Aβ load and tau pathology, enhanced neuroplasticity, reversed molecular signatures of anxiety, and ultimately improved memory and reduced fear.

Discussion: Kallikrein-8 is a promising new therapeutic target against AD.

Keywords: Alzheimer's disease; Kallikrein-8; Intraventricular antibody delivery; Ephrin receptor B2; Anxiety; Neuroplasticity; Aβ pathology; Aβ clearance; Autophagy; tau pathology

1. Introduction

Kallikrein-8 (KLK8, also known as neuropsin) is a synaptic plasticity-modulating extracellular serine protease [1,2]. Among other substrates KLK8 cleaves the ephrin receptor B2 (EPHB2) and thereby induces various signaling cascades. For instance in the amygdala, EPHB2 cleavage by KLK8 induces the expression of FK506-binding protein-5 (FKBP5), which in turn regulates glucocorticoid receptor sensitivity and provokes anxiety [3]. EPHB2 signaling via trans-cellular communication with ephrin B2 ligand (EFNB2) is further of particular relevance for neuronal plasticity, as it coordinates axonal guidance [4] and controls synaptogenesis [5]. EPHB2 signal transduction is also known to induce angiogenesis [6] and autophagy [7,8] under neoplastic conditions.

Given that all the aforementioned behavioral, molecular, and structural processes, that is, anxiety and cognition, neuronal [9,10], and vascular [11,12] plasticity, as well as autophagy [13,14] are also impaired in Alzheimer's disease (AD) patients and transgenic mice, it seems likely that KLK8/EPHB2 signaling could be involved in the pathogenesis of AD, although hitherto very few studies

Arne Herring and Kathy Keyvani are, since 25th of September 2015, inventors on a pending patent for KLK8 inhibitors. All authors have declared that no further biomedical financial interests or potential conflicts of interest exist.

*Corresponding author. Tel.: +49 201 723 3321; Fax +49 201 723 5927.
**Corresponding author. Tel.: +49 201 723 3334; Fax: +49 201 723 5927.
E-mail addresses: kathy.keyvani@uk-essen.de (K.K.), arne.herring@uk-essen.de (A.H.)

http://dx.doi.org/10.1016/j.jalz.2016.05.006

support this hypothesis. *KLK8* mRNA [15] is up-regulated in AD-affected human hippocampus, and hippocampal EPHB2 is reduced in AD patients and in *hAPP* mice [16,17]. Lentivirus-mediated EPHB2 up-regulation improves cognition [18] and ligand-triggered EPHB2 activation diminishes tau phosphorylation [19] in transgenic mice. Based on these fragmentary results, we hypothesized that inhibition of KLK8 and thereby reversing KLK8/EPHB2 imbalance would mitigate AD pathology. Here, we demonstrate a considerable up-regulation of KLK8, prior and in addition to EPHB2 depletion, in human and murine brain at incipient stages of AD, long before the "clinical" signs of disease appear. We further show that 4 weeks of KLK8 inhibition, by intraventricular delivery of an anti-KLK8 antibody after disease onset, is sufficient to mitigate multiple features of Alzheimer's pathology in transgenic mice. Our data strongly suggest that antibody treatment against KLK8 should be tested in clinical trials for its potential against AD.

2. Methods

2.1. General

All data presented in this article were generated in blind-coded experiments, in which the investigators who collected the data were unaware of the specific genotype and treatment of mice, brain slices, and cell cultures. Protein, peptide, and mRNA levels were quantified individually in duplicates or triplicates in separate brain areas from mice and humans.

2.2. Descriptive approach

2.2.1. Murine samples

Female TgCRND8 mice (hemizygously carrying and over-expressing a double-mutant human APP 695 transgene [*hAPP*+/−] harboring the "Swedish" and "Indiana" mutations [KM670/671NL & V717F] under the control of the hamster Prion protein promoter) [20] as well as wild-type littermates from the hybrid C57BL/6-C3H/HeJ background strain were kept in standard housing in groups of 4 animals from postnatal day 30 (P30) until P360 in two independent batches. To minimize a biased effect of the parental genotype on the phenotype of the investigated mice, equal numbers of transgenic and wildtype mice were used per litter. Brains from both genotypes were harvested at P30 (early juvenile period, before the onset of Aβ pathology, n = 8 per genotype), P90 (around the onset of Aβ pathology, n = 8 per genotype), P210 (advanced stage of Aβ pathology, n = 8 per genotype), and P360 (full-blown stage of AD-like pathology, n = 8 per genotype). The brain regions vulnerable for AD pathology and linked with AD-related cognitive decline, that is, frontal cortex, entorhinal cortex, and hippocampus as well as the lesser and later affected cerebellum were isolated and used for DNA, RNA, and protein extraction (15,596-018, TRIzol-reagent, life technologies).

2.2.2. Human samples

Frozen frontal cortices (gyrus frontalis medius), entorhinal cortices, hippocampi, and cerebella from AD patients classified (by two neuropathologists) as CERAD [21] A/Braak & Braak [22] I–II (n = 12, 5 females, 7 males, 73.92 ± 1.94 years, postmortem interval (PMI) 35 ± 3.97 hours), CERAD B/Braak & Braak III–IV (n = 5, 5 females, 84 ± 2.42 years, PMI 27.38 ± 6.64 hours), CERAD C/Braak & Braak V–VI (n = 7, 4 females, 3 males, 79.71 ± 2.2 years, PMI 25.29 ± 5.2 hours) as well as from neurologically healthy young controls (n = 6, 3 per sex, 30.67 ± 2.97 years, PMI 31.33 ± 10.18 hours), and age-matched controls (n = 10, 5 per sex, 65.6 ± 2.62 years, PMI 28.5 ± 3.37 hours) were separately isolated and subjected to DNA, RNA, and protein extraction. A list of all human samples is available in Supplementary Table 1.

2.3. Characterization of the anti-KLK8 antibody

Binding of the inhibitory anti-KLK8 antibody (1:200, M021-3, MBL International) to recombinant human KLK8 (rhKLK8, 20 pmol/µl, 2025-SE-010, R&D Systems) and to KLK8 from mouse brain homogenate (20 µg/sample) was validated by immunoblotting. Specificity of the anti-KLK8 antibody has been reported before, demonstrating that it does not cross-react with other cerebral serine proteases, such as α-thrombin, trypsin, kallikrein, tissue plasminogen activator, or urokinase plasminogen activator [23]. EPHB2 fragmentation by KLK8 was tested by incubation of recombinant chimeric EPHB2-FC (400 ng at 100 ng/µl, E9402, Sigma-Aldrich) with lysyl endopeptidase (0.01 A U./µg rhKLK8, 125-02,543, Wako) activated rhKLK8* (4 ng at 1 ng/µl) and subsequent EPHB2 immunoblotting (1:100, AF467, R&D Systems). The capacity of the anti-KLK8 antibody to protect EPHB2 from fragmentation was analyzed by incubation of 400-ng EPHB2-FC with 4-ng rhKLK8* which was blocked by pre-treatment with 80 ng anti-KLK8 antibody (at 20 ng/µl, rhKLK8*-block) in comparison to incubation of EPHB2-FC with rhKLK8* which was pre-incubated with 80-ng isotype control rat IgG (MCA1124R, AbD Serotec) and subsequent EPHB2 immunoblotting.

2.4. Experimental manipulations

2.4.1. In vivo *approach*

2.4.1.1. Intraventricular anti-KLK8 antibody delivery

A total of 16 female transgenic mice and 16 female wild-type littermates were standard housed in groups of 4 mice from P30 until P150 in 3 independent batches. At P150, all mice were subjected to subcutaneous implantation of osmotic pumps (7147160-6, Alzet 2004, Durect) and brain infusion kits (0008859-2, Alzet Brain Infusion Kit 3, Durect). A hole was drilled in the stereotaxically correct location (−0.2 Bregma, +0.9 parasagittal), and a cannula,

attached to the pump was inserted through the skull into the lateral ventricle and cemented in place, enabling constant intraventricular delivery of the anti-KLK8 antibody (M021-3, 62 μg/kg/d at an average concentration of 0.21 μg/μl diluted in saline and a flow rate of 0.25 μl/h, n = 8 per genotype), control rat IgG (MCA1124R, n = 7 per genotype), or saline (n = 1 per genotype) over a 4-week period. Antibodies were dialyzed against sterilized PBS, pH 7.4 to remove NaN_3 (88,401, Slide-A-Lyzer Mini Dialysis Devices, Thermo Scientific) before injection into pumps. To minimize a biased effect of the parental genotype on the phenotype of the experimental mice, littermates were equally distributed to verum and control groups.

2.4.1.2. Behavioral phenotyping

From P178 until P184, mice were behaviorally phenotyped. Before testing, they had been adapted to the inverted day/night cycle for 1 week. First, anxiety behavior was evaluated in the Elevated-Plus Maze (EPM) according to Young et al. [24]. The EPM consisted of two opposite open arms (each 27.5 × 6 × 0.5 cm, length × width × height), two opposite closed arms (each 27.5 × 6 × 16 cm) and a center platform (5 × 5 × 0.5 cm). The maze was 75 cm elevated above the ground. Each mouse was placed in the center and observed for 5 minutes. Number of entries, latencies until first time entries, duration and distance covered in closed and open arms, and in the center as well as velocity were automatically tracked and analyzed by Video Mot 3D software (TSE, version 7.0.1). The next day, mice were tested in the open field (OF) for exploratory behavior and general activity according to Kilic et al. [25]. The OF arena (52 × 52 × 30 cm) was located 72 cm above the floor on a circular platform. Each mouse was placed near the wall and observed for 10 minutes. The test arena was divided into one center (31.2 × 31.2 cm), four border (each 10.4 × 31.2 cm), and four corner (each 10.4 × 10.4 cm) areas. Number of entries, latencies until first time entries, duration, and distance covered in each area as well as velocity were automatically tracked. From P180 until P184, hippocampus-associated spatial memory and learning performance was assessed by the Barnes Maze (BM) according to Sunyer et al. [26]. The BM arena consisted of a circular platform (92 cm diameter, 120 cm above the ground) with 20 equally distributed holes (5 cm diameter, 7.5 cm distance between holes) located at the border. One hole (escape hole) was connected to a box (15.5 × 9.5 × 6 cm), allowing to escape from the BM platform, whereas the other 19 holes were closed (error holes). Twenty four hours before tests started, mice were habituated to the setup for two trials, each lasting for 3 min. Tests were performed between 10:00 am and 6:00 pm. Each mouse was placed in a black cylinder located in the middle of the platform for 10 seconds. During that time, red light was switched to bright light (180 lx), and the cylinder was lifted, defining the start of a 3-minute trial. During each trial, primary errors, total errors, primary latency, total latency, path length covered, and velocity were automatically recorded. Primary errors and latencies were defined as the number and duration of approximations to error holes until approaching the escape hole for the first time. Total errors and latencies were defined as the number and duration of approximations to error holes and to the escape hole until final escape. Once a mouse escaped, it was allowed to stay in the escape box for 1 minute before being transferred to the home cage. If a mouse did not escape during the 3-minute interval, it was gently guided to the escape hole until the mouse escaped; otherwise, it was placed directly into the escape box for 1 minute. On test day 1, each mouse was tested in four trials. On test days 2, 3, 4, and 5, each mouse was tested in two trials. Inter-trial intervals lasted for 15 minutes. After the four test days, the escape hole was blocked at day 5 (probe trial). Mice were allowed to explore the platform for 90 sec per trial. In all behavioral tests, freezing and exploration behavior were manually recorded. Before and after each test, the EPM, OF, and BM arenas were cleaned with 70% ethanol.

2.4.1.3. Blood and tissue sampling

After behavioral testing, blood was collected from retrobulbar venous plexus of each transgenic animal to determine baseline circulating plasma Aβ levels. To quantify Aβ efflux efficacy across the brain-blood barrier (BBB), 7 anti-KLK8 antibody-treated, 6 IgG treated, and 1 saline-treated transgenic mouse received an intravenous (tail vein) injection of an Aβ stabilizing anti-Aβ antibody (HJ5.1, 150 μg/animal) (purchased from Dr. David M. Holtzman's laboratory, St. Louis, Missouri [27]) that only marginally enters brain parenchyma and does not affect the Aβ-brain-to-blood-equilibrium to prevent the naturally occurring rapid Aβ degradation in blood ($t_{1/2}$ = 2–3 minutes) which precludes a direct and sensitive quantification of brain-derived Aβ over baseline circulating plasma Aβ. 1 anti-KLK8 antibody-treated versus 1 IgG-treated transgenic mouse received saline as control. 10 and 40 minutes after HJ5.1-antibody or saline injection, blood was collected again. Pump implantation, intravenous injection, and retrobulbar venous blood collection was conducted in anesthetized mice with 2% isoflurane in oxygen/nitrous oxide (20%:40%) using a vaporizer. Afterward, mice were sacrificed (in deep anesthesia). Frontal cortex, hippocampus, amygdala (basolateral & central nuclei), and basal ganglia were isolated and separately homogenized from one hemisphere. Homogenates were subjected to DNA, RNA, and protein extraction (TRIzol-reagent). From the remaining intact hemisphere, the frontal pole (+4 to +1.5 Bregma) was impregnated with Golgi-Cox solution (PK401-A, FD Rapid GolgiStain Kit, FD NeuroTechnologies) and subsequently cut into 200-μm coronal sections. The rest of the brain hemisphere was formalin-fixed, paraffin-embedded, and cut into 10-μm coronal sections for immunohistochemistry.

2.4.2. In vitro *approach*

Between 14 days *in vitro* (DIV 14) and DIV 21, primary mixed glial cell cultures (50%:50% microglia:astroglia) from whole cerebrum of neonatal (P0) transgenic or wildtype mice were characterized for the presence of extracellular and intracellular KLK8 (1:200, ABIN759116, antibodies-online.com) and for intracellular EPHB2 (1:100, AF467) via immunoblot as well as for intraglial and extraglial $A\beta_{40}$ and $A\beta_{42}$ by ELISA ($A\beta_{40}$ and $A\beta_{42}$, KHB3482 and KHB3442, Invitrogen).

At DIV17, primary mixed glia (50%:50% microglia:astroglia, 250,000 cells per well for lysates, 60,000 cells per well for immunofluorescence cytochemistry, 100,000 cells per well for autophagy monitoring, 150,000 cells per well for cell viability monitoring) were incubated either with anti-KLK8 antibody (M021-3) or control IgG antibody (MCA1124R) at a concentration of 5 μg/mL (dialyzed against PBS as described above). At DIV18, $A\beta_{42}$ (100 ng/mL, 72,071, SensoLyte Fluorescent $A\beta_{42}$ Sampler Kit, Anaspec) as well as fresh antibody (2.5 μg/mL) were added to the medium (41,966–029, DMEM, 16,050–122, 10% horse serum, 15,140–122, 1% penicillin/streptomycin, all from Thermo Fisher Scientific). At DIV19 and DIV20, antibody but not $A\beta_{42}$ treatment was repeated. Supernatant and cell lysates were collected at DIV 17 to DIV 21. To test whether effects of anti-KLK8 antibody treatment were transduced by the EPHB2 receptor, we simultaneously co-incubated anti-KLK8-treated glial cells with an inhibitory anti-EPHB2 antibody (2 μg/mL, AF467, R&D Systems) (for experimental setting see also Supplementary Fig. 4A).

2.5. *Outcome measures*

2.5.1. *Descriptive approach*

Protein levels of EPHB2 (1:100, AF467), EFNB2 (murine: 1:500, AF496, R&D Systems; human: 1:100, ab96264, abcam), KLK8 (1:100, ABIN759116), FKBP5 (murine: 1:500, human: 1:200, ab2901, abcam), beclin-1 (1:2,000, ab62557, abcam), and STX17 (1:1,000, 17,815-1-AP, Acris) were quantified by immunoblot. Protein levels of GAPDH (1:15,000, G9545, Sigma-Aldrich), actin β (1:15,000, A5441, Sigma-Aldrich), or determination of total protein load via fluorescent gel electrophoresis (TGX stain free gels, 161-0183, Bio-Rad) served for normalization. Transcription levels of murine and human *KLK8*, *FKBP5*, *EPHB2*, and *EFNB2* were measured via quantitative real-time PCR (TaqMan assays, ABI 7500 Fast real-time PCR cycler, Applied Biosystems) after reverse transcription of DNase-treated RNA extracts to cDNA (ABI High-Capacity RT Kit, #4368814, Applied Biosystems) and normalized against *GAPDH* or cytochrome c1 (*CYC1*). Intron-spanning forward and reverse primer sequences and the TaqMan probe forward sequences are available on request.

2.5.2. In vivo *approach*

Sufficient cerebral penetration of anti-KLK8 antibody or control IgG antibody (both antibodies produced in rat) after intraventricular delivery was validated in lysates from frontal cortex, basal ganglia, hippocampus, and amygdala by visualization of rat immunoglobulins with secondary anti-rat-HRP antibody (1:5000, A9037, Sigma-Aldrich) via immunoblotting.

Protein levels of EPHB2 (1:100, AF467), synaptophysin (1:10,000, M7315, DAKO), GAP43 (1:4000, GTX11136, GeneTex), ARC (1:500, sc-15325, Santa Cruz Biotechnology), FKBP5 (1:500, ab2901), glucocorticoid receptor (1:1000, ab109022, abcam), APP (and the processing fragment CTFβ, 1:2000, A8717, Sigma-Aldrich), MDR1 (1:1000, APO94346PU-N, Acris), LRP1 (1:500, 438192, Calbiochem), RAGE (1:1000, SP5151P, Acris), beclin-1 (1:2000, ab62557, abcam), ATG5 (1:500, A0856, Sigma-Aldrich), STX17 (1:1000, 17,815-1-AP, Acris), cathepsin D (1:1000, ab6313, abcam) and prostaglandin E receptor 2 (1:500, APO01201PU-N, Acris) were determined by immunoblotting. GAPDH served for normalization. Tau phosphorylation levels at amino acids S202/T205 (1:500, AT8, MN1020, Thermo Scientific), S396 (1:1000, PA5-35455, Thermo Scientific) and T212/S214 (1:500, AT100, MN1060, Thermo Scientific), PI3K phosphorylation at T199/T458 (1:2,000, #4228, Cell Signaling Technology), Akt phosphorylation at S473 (1:1000, #9271, Cell Signaling Technology), GSK3β phosphorylation at S9 (1:1000, #9336, Cell Signaling Technology) and total protein levels of tau (1:500, tau-5, MAB361, Millipore), PI3K (1:500, #4257, Cell Signaling Technology), Akt (1:1000, #9272, Cell Signaling Technology), and GSK3β (1:2000, #9315, Cell Signaling Technology) were quantified by immunoblotting as well. Total protein levels of tau, PI3K, Akt, and GSK3β as well as GAPDH served for normalization.

sAPPα (JP27734, IBL International), $A\beta_{40}$, and $A\beta_{42}$ peptide levels were quantified by ELISA in protein homogenates containing 1% SDS.

Transcription levels of *hAPP* were determined via quantitative real-time PCR and normalized against *GADPH* mRNA levels. Primer and TaqMan probe sequences are available on request.

For morphometric analyses, a Nikon 80i microscope with an integrated CFI ocular lens (10× magnification), equipped with CFI PLAN ACHROMAT objectives (2× magnification, numerical aperture 0.06; 10× magnification, numerical aperture 0.25), CFI PLAN FLUOR objectives (20× magnification, numerical aperture 0.5; 40× magnification, numerical aperture 0.75) and a PLAN APOCHROMAT VC objective (100× magnification, numerical aperture 1.4) (all objectives from NIKON), a color digital camera (3/4″ chip, 36-bit color, DV-20, MicroBrightField), and MicroBrightField software were used. Aβ plaques (1:100, 6F/3D, DAKO), microglia (AIF1, 1:100, APO8912PU-N, Acris), and cerebral vessels (laminin, 1:300, L9393, Sigma-Aldrich) were visualized and stereologically quantified in 10 sections (with 100 μm inter-

space between sections) per staining and animal as previously described [28] with minor modifications. Briefly, Aβ plaque load was quantified at 200× magnification. Aβ plaque volume (i.e., percentage of cerebral volume covered by deposits) and Aβ plaque number (n/mm^2) were calculated in an unbiased manner by area fraction fractionator and fractionator (counting frame and grid size, each 500 × 500 μm), respectively. The number of microglia with a visible soma and blood vessel bifurcations (n/mm^2) [(vessel ends + vessel branch point)/2] were determined at 200× magnification via fractionator (counting frame 250 × 250 μm, grid size 375 × 375 μm). Additionally, 6 sections per animal were co-stained for Aβ plaques and microglia. The average number of plaques surrounding microglia was calculated using the fractionator probe (counting frame 250 × 250 μm, grid size 375 × 375 μm) at 200× magnification. Absolute values were related to the investigated area (Stereo Investigator 11, MicroBrightField). Six sections per animal were co-stained for Aβ plaques and phosphorylated tau (1:80, AT8, MN1020, Thermo Scientific). To determine the proportion of neuritic plaques, the number of AT8-positive Aβ plaques was set in relation to the total number of Aβ plaques (with or without surrounding AT8-positive neurites) using the fractionator probe (counting frame, 250 × 250 μm; grid size, 375 × 375 μm) at 200× magnification.

The effect of KLK8 inhibition on structural neuronal plasticity was tested in Golgi-Cox impregnated coronal sections. We analyzed 10 pyramidal neurons from layer V frontal cortex (+4 to +1.5 Bregma) per animal. All apical and basal dendrites extending from the neuron soma were traced (Neurolucida 11, MicroBrightField) at 400× magnification for 3D reconstruction. To determine dendritic spine density, spines were counted on four 20-μm long dendritic segments per neuron, i.e. on a proximal apical segment, on a distal apical segment, on a proximal basal segment, and on a distal basal segment at 1000× magnification. A proximal segment was defined to start after the first dendritic branch point, a distal one after the third branch point. To quantify apical and basal dendritic morphology, a morphometric analysis of dendritic number, length, and branching complexity was performed. Dendritic complexity was calculated by the formula: [sum of the terminal orders + number of terminals] × [total dendritic length/number of primary dendrites]; with terminals defined as dendritic endings and the terminal order defined as the number of "sister" branches encountered while proceeding from the terminal to the cell body (NeuroExplorer, MicroBrightField).

2.5.3. In vitro *approach*

The influence of anti-KLK8 antibody on glial EPHB2 protection was validated by quantification of EPHB2-FL in lysates using immunoblotting (1:100, AF467).

Anti-KLK8 antibody triggered autophagy modulation was determined by beclin-1 (1:500, ab62557), ATG5 (1:500, A0856, Sigma-Aldrich), and STX17 (1:1,000, 17,815-1-AP) immunoblot and via an autophagy assay (600140, autophagy/cytotoxicity dual staining kit, Cayman Chemical) after manufacturer's instructions analyzed on a fluorescence microplate reader (Flx800, BioTek).

Aβ phagocytosis was determined by quantification of $A\beta_{42}$ in glial lysates and supernatant by ELISA and microglial $A\beta_{42}$ uptake visualized by fluorescent $A\beta_{42}$ and AIF1 immunofluorescence cytochemistry (1:100, APO8912PU-N, Acris Antibodies).

Cell viability was monitored after manufacturer's instructions (9095S, XTT cell viability kit, Cell Signaling Technology). Wildtype and transgenic cells were examined separately. Owing to lack of significant differences, data of both genotypes were pooled.

2.6. Statistics

Data are presented as means ± SE. Distribution of all data sets was evaluated by 1-sample Kolmogorov–Smirnov test and Q-Q plots. Homogeneity of variance was calculated with the Levene test. Student *t* test with Bonferroni correction for multiple testing was applied for the analyses of two groups. For the descriptive approach, multiple groups comparison was analyzed by 2-way analysis of variance (ANOVA) with aging (in mice: P30–P360, in humans: young vs. old) and murine genotype (transgene vs. wildtype) or human disease status (AD vs. control) as between-subject factors and Bonferroni *post hoc* test. For the experimental *in vivo* approach, multiple groups' comparison was analyzed by 2-way ANOVA with treatment (verum vs. control) and genotype (transgene vs. wildtype) as between-subject factors and Bonferroni *post hoc* test. Cell culture experiments were analyzed by 2-way ANOVA with treatment (verum vs. control) and time as between-subject factors and Bonferroni *post hoc* test. Pearson-correlation analysis was performed to test the strength of association between protein levels of KLK8/EPHB2 signaling members. A significance level (α) of $P < .05$ was selected. All tests were performed using the software package SPSS 22 (IBM).

2.7. Ethical considerations

All animal experiments were carried out in accordance with the EU Directive 2010/63/EU for animal experiments. Permission for mice breeding and decapitation (AZ 84-02.04.2014.A488) as well as for animal experiments (G1338/12; AZ 84-02.04.2012.A412) was granted by the local committee LANUV NRW, Germany.

Using postmortem human material was approved by the ethics committees of the Medical Faculties, University of Duisburg-Essen, (14-5861-BO) and Ludwig-Maximilians-University Munich (#345-13), Germany. Written informed consent was received from the family members of the dead patients before inclusion in the study.

3. Results

3.1. KLK8 overexpression in precursor stages of AD

First, we assessed the temporal and spatial mRNA and protein expression patterns of KLK8, and its downstream cascade members EPHB2, FKBP5, and EFNB2 during the course of AD progression in the hippocampus, frontal cortex, entorhinal region, and cerebellum of both transgenic CRND8 and wildtype mice as well as AD patients and in neurologically healthy (young and old) controls. In particular, in the hippocampus (Fig. 1), KLK8 protein levels were increased long before disease onset at P30 in transgenic mice (Fig. 1A and 1B) when compared to age-matched controls. Presumably due to decline of neuroplasticity processes in the aging brain, there was an age-related KLK8 drop in both mouse genotypes (reaching a steady state level in transgenics after P90 and in wildtypes after P210). In spite of this drop, KLK8 levels remained throughout all ages almost constantly higher in transgenics than in wildtypes. In AD patients, hippocampal KLK8 levels were already higher at CERAD A/Braak I–II stage when compared to aged-matched controls (Fig. 1C and 1D); KLK8 level increased further with AD progression (CERAD A/Braak I–II to CERAD C/Braak V–VI, Fig. 1C and 1D). Owing to lack of appropriate samples, we cannot make any statements on the course of KLK8 expression in severer stages of pathology in mice (e.g., in P540 or older), and it remains also unclear whether KLK8 levels are, as it is the case in mice, already elevated in infant brains of future AD patients. It is tempting to speculate that this, at least in familiar AD cases could be true. A disease-related KLK8 overabundance could be detected also in other brain regions, that is, the frontal cortex, entorhinal cortex, and even cerebellum (Supplementary Fig. 1) of both species. KLK8 overexpression was followed by a reduction of full-length EPHB2 (EPHB2-FL) receptor levels in the hippocampus of transgenic mice at P210 (Fig. 1A and 1B) and in patients with moderate AD at CERAD B/Braak III–IV stage (Fig. 1C and 1D). EPHB2 levels declined also in the murine cerebellum and human frontal cortex but not in the entorhinal cortex (Supplementary Fig. 1). FKBP5 protein levels were elevated in the frontal, entorhinal, and cerebellar cortex (Supplementary Fig. 1) as well as in the hippocampus very early at P30 in transgenic mice and at CERAD A/Braak I–II stage in humans but declined during the course of disease (Fig. 1A–1D). EPHB2 ligand EFNB2 was down-regulated during disease progression, in the murine hippocampus (Fig. 1A and 1B) and displayed reduced entorhinal and cerebellar levels, only in the later stages of disease in mouse (P210) and man (CERAD C; Supplementary Fig. 1).

The exceedingly early and multifocal up-regulation of the protease KLK8, even in the scarcely AD-affected cerebellum not only explains the subsequent decline of its proteolytic target EPHB2 (supported also by a strong negative correlation between hippocampal KLK8 and EPHB2 protein levels, $r = -0.663$, $P < .001$) but also suggests a causal role in the cascade of events leading to AD. We therefore sought to verify whether inhibiting the proteolytic enzyme KLK8 would mitigate Alzheimer's pathology.

3.2. Anti-KLK8 antibody inhibits KLK8 activity

We first confirmed that anti-KLK8 antibody, but not the isotype control IgG, specifically (i.e., with no cross-

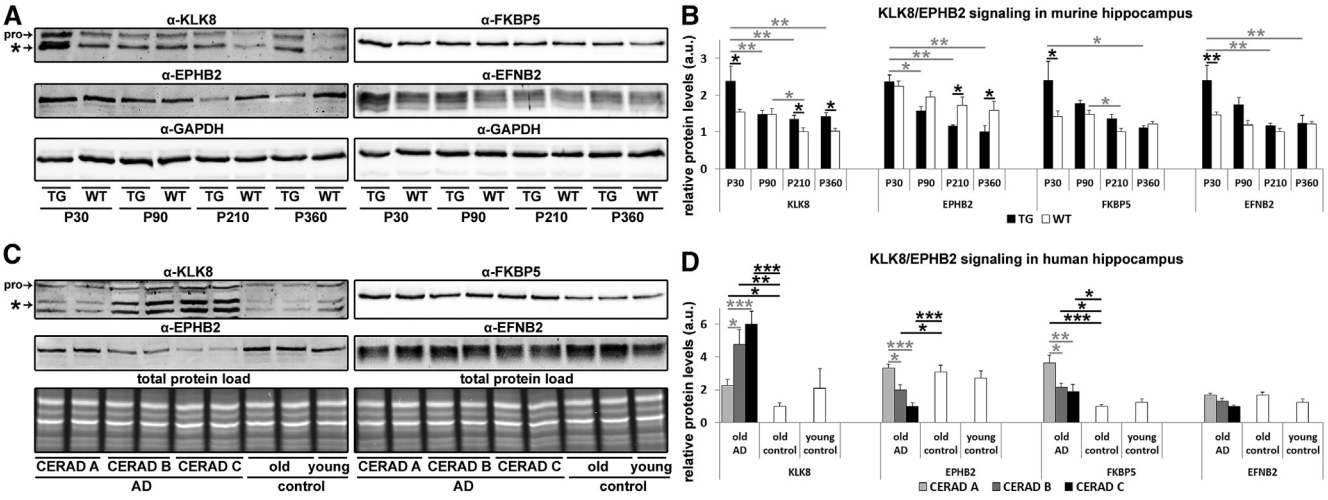

Fig. 1. KLK8 overexpression at incipient stages of AD precedes the depletion of its proteolytic target EPHB2. (A–B) Hippocampal expression of KLK8, EPHB2, FKBP5, and EFNB2 in young (P30), adolescent (P90), adult (P210), and old (P360) transgenic (TG) and wildtype (WT) mice. (C–D) Hippocampal expression of KLK8, EPHB2, FKBP5, and EFNB2 in AD patients at CERAD A/Braak I–II, CERAD B/Braak III–IV, CERAD C/Braak V–VI stages, and young and old controls. A combined quantification of the pro-form of KLK8 and activated KLK8* is depicted for murine and human samples. *$P < .05$, **$P < .01$, ***$P < .001$ (2-way ANOVA and Bonferroni *post hoc* test). Black asterisks indicate comparison between diseased and control groups, gray asterisks indicate comparison between different disease and age stages within diseased or control groups. $n = 8$ per murine group and $n = 5$–12 per human group. Results are shown as mean ± SEM.

reactivity with other serine proteases [23]), binds to human and murine KLK8 (Supplementary Fig. 2A). The functionality of this antibody was tested by examining the cleavage efficiency of KLK8 on its substrate EPHB2 whose processing results in a 70-kDa extracellular, N-terminal fragment (EPHB2-NTF) [3]. After proving that EPHB2 is cleaved by KLK8 in a cell free *in vitro* assay (Supplementary Fig. 2B and 2C), we demonstrated that the anti-KLK8 antibody is able to protect EPHB2 from fragmentation both in the cell free assay (Supplementary Fig. 2B and 2C) and in primary glial cell culture (Supplementary Fig. 2D and 2E). To test the inhibitory efficacy of the anti-KLK8 antibody *in vivo*, anti-KLK8 antibody, control IgG, or saline was intraventricularly delivered over a 4-week period to 150-day old transgenic and wildtype mice using osmotic pumps (for experimental setting see also Fig. 2A). After confirmation of sufficient cerebral antibody penetration (Supplementary Fig. 2F), quantification of EPHB2-FL revealed that anti-KLK8 antibody treatment successfully blocked EPHB2 cleavage (Supplementary Fig. 2G and 2H). During the treatment period, none of the mice exhibited any signs of adverse reaction. Body mass were not affected by treatment (data not shown).

3.3. KLK8 inhibition reduces fear and improves cognition

Progressive cognitive decline and increased anxiety are the clinical hallmarks of AD. Previous studies demonstrated that KLK8-triggered amygdalar EPHB2 fragmentation controls anxiety [3], that lentivirus-mediated EPHB2 up-regulation reduces cognitive impairment in transgenic AD mice [18] and that high concentrations of KLK8 impair hippocampal long-term potentiation and induce long-term depression *ex vivo* [29]. We therefore postulated that cerebral KLK8 inhibition (and subsequent EPHB2 protection) might exert anxiolytic effects and improve memory performance in transgenic brains characterized by abnormally high KLK8 levels. Accordingly, after 4 weeks of antibody delivery, mice were phenotyped for anxiety-related behavior in the EPM, for avoidance and exploratory behavior in the OF and for spatial memory in the BM; for experimental design see Fig. 2A. Automated video tracking analysis substantiated that antibody-mediated cerebral KLK8 inhibition has anxiolytic effects and increases exploratory behavior in transgenic mice, as anti-KLK8 antibody-treated animals spent more time in the open arms and less time in the closed arms of the EPM (Fig. 2B and 2C), spent more time in the center and border areas and less time in the corners of the OF arena (Fig. 2E and 2F), took less time to enter the center area for the first time (Fig. 2H), and showed reduced freezing and increased exploratory behavior (Fig. 2I), when compared to controls (IgG & saline). Evaluation of the BM further revealed that blockade of KLK8 improved spatial memory performance in AD-affected mice, as verum-treated transgenics had reduced latencies (Fig. 2J–2L), explored fewer wrong holes (Fig. 2M and 2N), and covered shorter distances (Fig. 2O and 2P) before escaping through the escape hole at trial 1 on test day 1 (24 hours after 2 trials of habituation) as well as on test day 4. Cognitive improvement through KLK8 blockade was not accompanied by changes in motor skills, as the average speed did not differ between the two transgenic groups (data not shown). Wildtype control mice (treated with IgG or saline) showed less anxiety, more exploration activity (Fig. 2B–2I), and better cognitive performance (Fig. 2J–2P) when compared to transgenic control mice. In contrast to the positive effects of anti-KLK8 antibody administration to transgenics, wildtype mice barely benefited from this treatment. Although anti-KLK8 treatment elicited anxiolytic effects also in wildtypes, as they spent less time in the closed arms of the EPM (Fig. 2B and 2C) and exhibited increased exploratory behavior in the OF (Fig. 2E and 2I), their memory performance deteriorated significantly in the BM. Verum-treated mice showed increased latencies (Fig. 2J–2L), explored more wrong holes (Fig. 2M and 2N), and covered longer distances (Fig. 2O and 2P) before escaping through the escape hole at trial 1 on test day 1 and on test day 4. Cognitive impairments were accompanied by a tendency to hyperactivity, indicated by increased total distance travelled in the EPM, OF, and BM arenas (Fig. 2D and 2G, P). The mild adverse reactions occurring in wildtypes (expressing KLK8 at physiological levels) underlines, that only individuals with pathological high KLK8 levels benefits from this therapy. This is in line with a previous study which has demonstrated that KLK8 reduction beneath or rise above physiological levels both impairs spatial memory performance in wildtype mice [29].

3.4. KLK8 inhibition reverses the molecular signatures of anxiety and enhances structural neuroplasticity

Next, we verified the effect of anti-KLK8 antibody treatment on molecular and structural signatures of anxiety and cognition. The first step was to quantify the protein levels of anxiety-modulating FKBP5 and glucocorticoid receptor in the amygdala (as published in [3]) and in the frontal cortex (an area which is not ostensibly involved in anxiety control). In line with the anxiolytic effect of KLK8 inhibition, anti-KLK8 antibody treatment strongly suppressed FKBP5 and glucocorticoid receptor expression in the amygdala of both transgenic and wildtype mice (Fig. 3A and 3B). In the frontal cortex, antibody administration influenced neither FKBP5 nor glucocorticoid receptor expression (Fig. 3C and 3D). In the next step, we measured the protein levels of structural neuroplasticity markers synaptophysin (SYP), GAP43, and ARC in the hippocampus and frontal cortex. In both transgenic (but not wildtype) brain areas, KLK8 inhibition increased the expression of the synaptogenesis and growth cone markers SYP and GAP43 (but not ARC, Fig. 3E–3H). Accordingly, we determined the

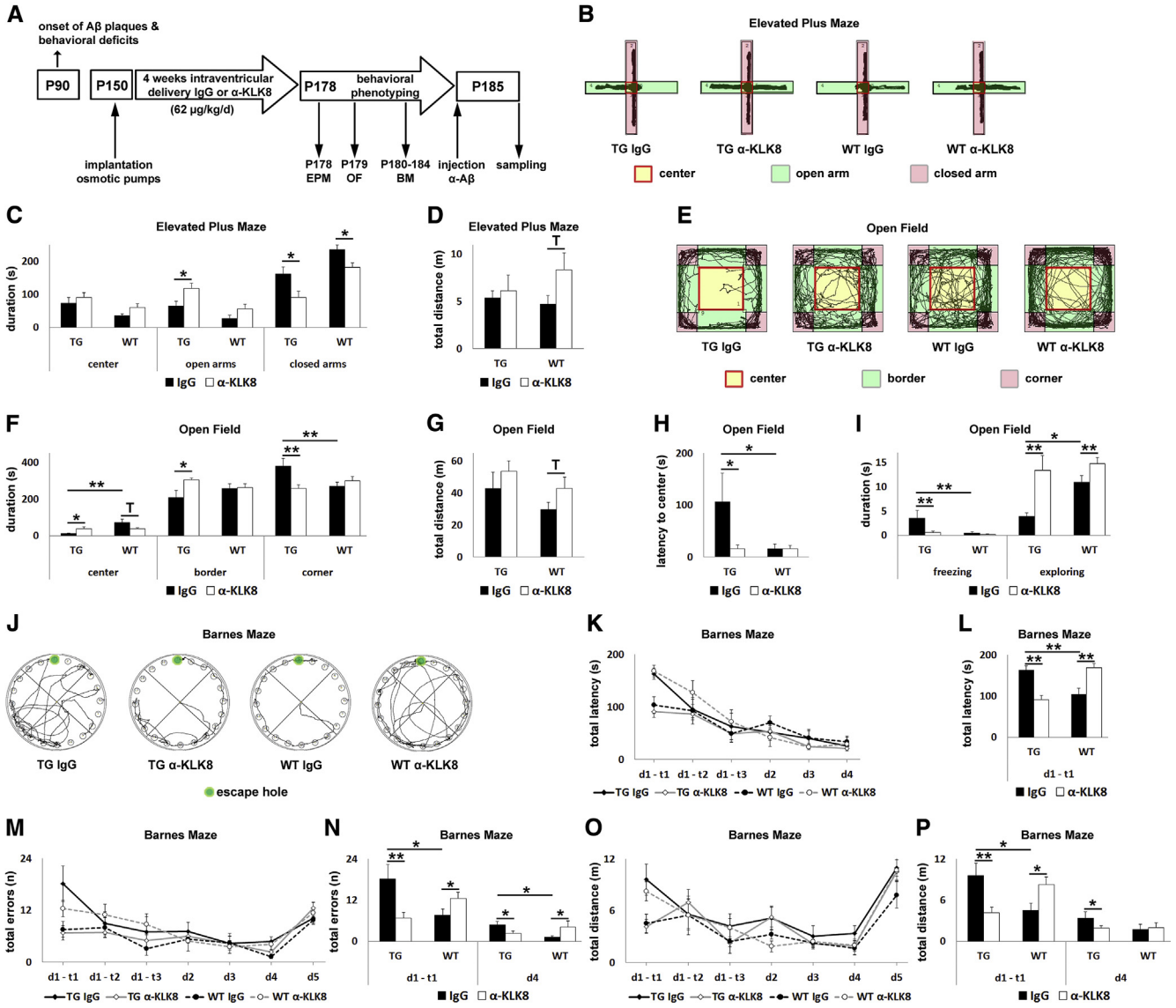

Fig. 2. KLK8 inhibition reduces fear and improves cognition. (A) Anti-KLK8 treatment scheme. At P150 (2 months after disease onset), 16 female transgenic (TG), and 16 female wildtype (WT) mice were subjected to subcutaneous implantation of osmotic pumps, enabling constant intraventricular delivery of either the anti-KLK8 antibody (α-KLK8) (n = 8 per genotype), IgG (n = 7 per genotype), or saline (n = 1 per genotype) over a 4-week period. At P178, mice were tested in the Elevated-Plus Maze (EPM) for anxiety, at P179 in the Open Field (OF) for exploratory behavior and between P180 and P184 for spatial memory and learning performance in the Barnes Maze (BM). At P185, TG mice received an intravenous injection of an anti-Aβ antibody (α-Aβ) or saline, followed by blood and brain tissue collection. (B, E, J) Representative paths from the EPM (B), the OF (E), and the BM (test day 1 [d1], trial 1 [t1], J). (C) Total time mice spent in the center area, open arms, and closed arms of the EPM platform. (D) Total distance mice travelled in all three compartments of the EPM. (F) Total time mice spent in the center area, borders, and corners of the OF platform. (G) Total distance mice travelled in all three compartments of the OF. (H) Time it took mice to enter the center area of the OF for the first time. (I) Total time mice showed freezing or exploring behavior in the OF. (K, M, O) Learning curves during spatial training in the BM. Total time (K, L), number of wrong holes approached (M, N), and total distance (O, P) mice needed to escape from the BM platform on d1–t1 and d4 (L, N, P). $^{T}P < .1$, $^{*}P < .05$, $^{**}P < .01$ (2-way ANOVA and Bonferroni *post hoc* test). $n = 8$ per genotype and treatment. Results are shown as mean ± SEM.

spine density and complexity of dendritic branching in Golgi-Cox-impregnated pyramidal neurons from layer V frontal cortex (using Neurolucida and Neuro Explorer software) and could corroborate increased spine density in anti-KLK8 antibody-treated transgenics (but not wildtypes; Fig. 3I$_{1\text{-}2}$, J), as well as elevated dendritic complexity after cerebral KLK8 blockade in both genotypes (Fig. 3I$_{3\text{-}6}$, K-M).

3.5. *KLK8 blockade counteracts Aβ pathology*

To determine whether blockade of KLK8 might reverse AD-related Aβ pathology, we investigated APP metabolism and Aβ plaque pathology in the frontal cortex and in the later and less affected basal ganglia. In both areas, four weeks of anti-KLK8 antibody administration increased APP-FL levels (without affecting the transcription of the *hAPP*

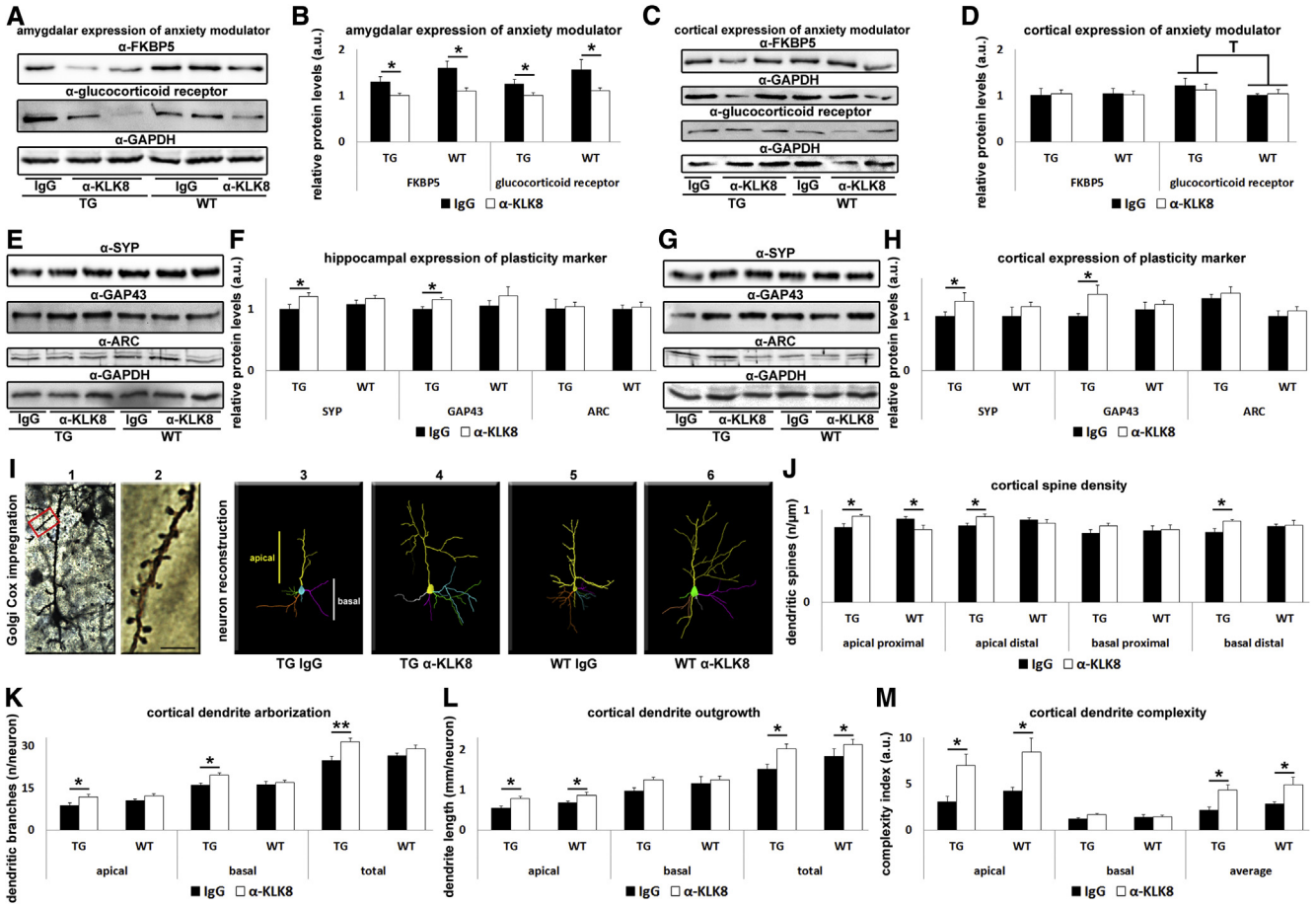

Fig. 3. KLK8 inhibition reverses the molecular signatures of anxiety and enhances structural neuroplasticity. Levels of anxiety-modulating FKBP5 and glucocorticoid receptor in the amygdala (A, B) and frontal cortex (C, D) of transgenic (TG) and wildtype (WT) mice treated with IgG or anti-KLK8 antibody (α-KLK8). Levels of structural plasticity markers SYP, GAP43, and ARC in the hippocampus (E, F) and frontal cortex (G, H) of TG and WT mice treated with IgG or α-KLK8. (I) Representative image of a Golgi-Cox-impregnated layer V frontal cortex neuron (image 1) and a magnified dendrite with spines (image 2) from the same neuron (indicate by the red rectangle). Scale bar: 5 μm. Representative images (images 3–6) of digital reconstructions from Golgi-Cox-impregnated neurons from all four murine groups. (J) Quantification of the average apical proximal and distal as well as basal proximal and distal spine density. The average number of branches (K), the average length (L), and the complexity index (M) of apical, basal, and total dendrites per neuron was determined in the same neurons. $^{T}P < .1$, $^{*}P < .05$, $^{**}P < .01$ (2-way ANOVA and Bonferroni *post hoc* test). $n = 8$ per genotype and treatment. Results are shown as mean ± s.e.m.

transgene), decreased APP C-terminal fragments β (CTFβ) and $A\beta_{42}$ peptide concentration, whereas $A\beta_{40}$ and sAPPα peptide levels remained unaffected (Fig. 4A–4E). These results indicate that blockade of KLK8 impedes amyloidogenic APP processing. We then tested whether changes in APP metabolism led to changes in Aβ plaque burden. Stereological quantification revealed that in the basal ganglia, KLK8 blockade diminished the total volume and average size (but not the total number) of diffuse Aβ plaques (which gradually evolve into core plaques) without affecting the load of the longer established core plaques, whereas in the frontal cortex, plaque load remained unchanged (Fig. 4F–4J). The fact that anti-KLK8 antibody treatment affected only those plaques with a younger history in the plaque ontogeny implies that KLK8 inhibition interferes with early steps in the amyloid cascade. Taken together, only 4 weeks of KLK8 inhibition is capable to suppress amyloidogenic APP processing and the subsequent Aβ production, thereby counteracting Aβ aggregation into diffuse plaques, at least in brain areas which are not yet tightly littered with amyloid deposits.

3.6. KLK8 inhibition improves neurovascular function

As EPHB2 induces angiogenesis [6], we hypothesized that cerebral KLK8 inhibition and the subsequent protection of EPHB2 from fragmentation might have improved the function of the neurovascular unit. Stereologic evaluation of cerebral blood vessel branching in the frontal cortex and basal ganglia (hereafter referred to as cerebral) revealed a pro-angiogenic effect of KLK8 inhibition, only in wildtype mice but not in the transgenics (Fig. 4K and 4L). Next, we determined the impact of KLK8 inhibition on the cerebral expression pattern of the BBB-located Aβ efflux-conducting LRP1 and MDR1 (also known as P-glycoprotein 1), and the Aβ influx receptor RAGE. RAGE did not change

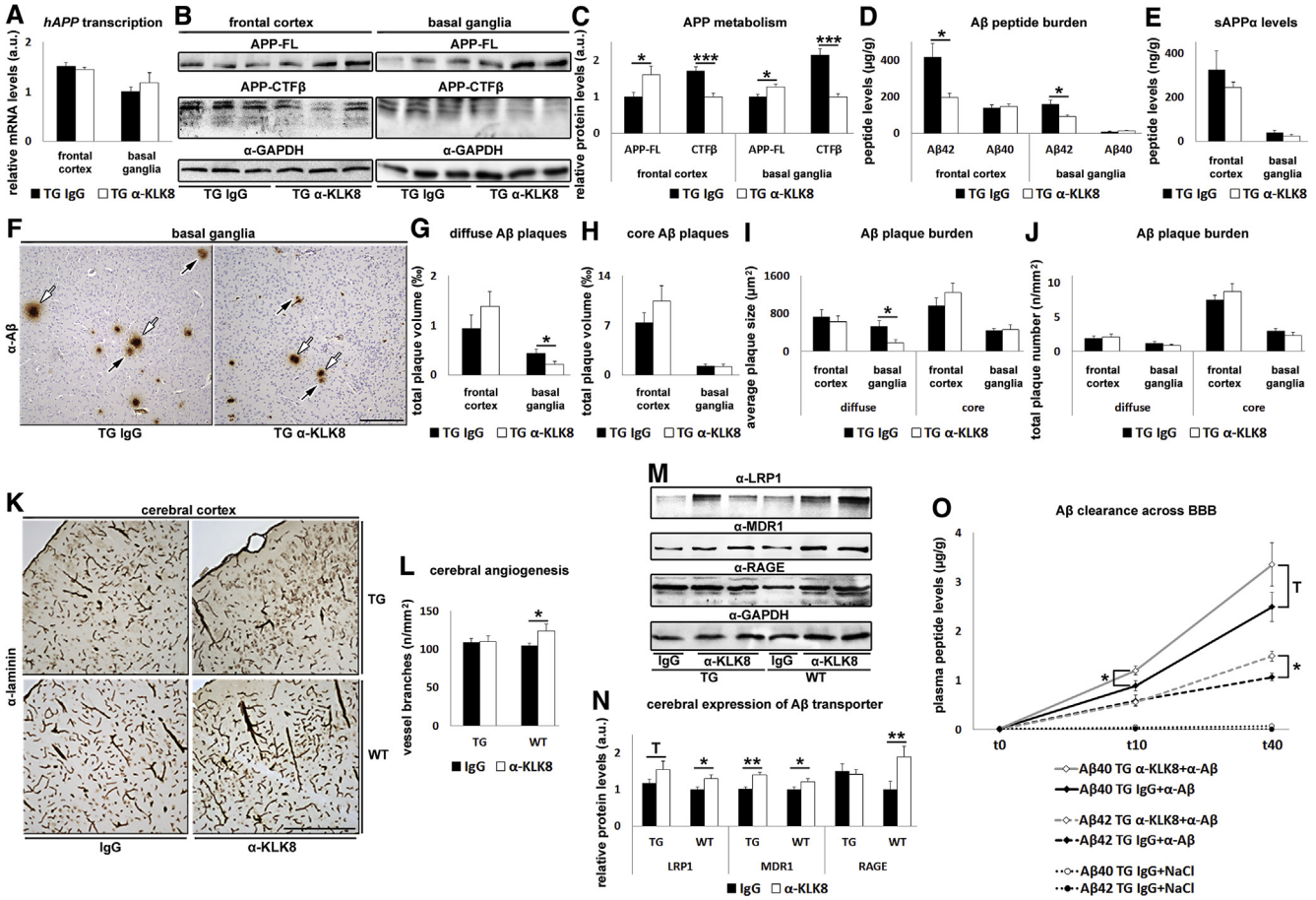

Fig. 4. Anti-KLK8 antibody treatment counteracts Aβ pathology and improves neurovascular function. (A) *hAPP* mRNA levels in the frontal cortex and basal ganglia of transgenic (TG) mice treated with IgG or anti-KLK8 antibody (α-KLK8). Full-length APP (APP-FL) and C-terminal fragment β (APP-CTFβ) levels (B, C), $Aβ_{42}$, and $Aβ_{40}$ (D), and sAPPα peptide levels (E) in the frontal cortex and basal ganglia of IgG or α-KLK8-treated TG mice. (F) Anti-Aβ immunostaining of basal ganglia showing diffuse (black arrows) and core (white arrows) Aβ plaque burden in TG IgG (left) and TG α-KLK8 (right) mice. Scale bar: 200 μm. Stereological quantification of total diffuse (G) and core (H) plaque volume, as well as of the average plaque size (I) and the total plaque number (J) in the frontal cortex and basal ganglia. (K) Representative cerebral anti-laminin immunostaining of TG and wildtype (WT) mice treated with IgG or α-KLK8. Scale bar: 100 μm. (L) Stereological quantification of cerebral (frontal cortex and basal ganglia) blood vessel branches. (M, N) Cerebral levels of Aβ transporters LRP1, MDR1, and RAGE from IgG or α-KLK8-treated TG and WT mice. (O) Aβ efflux dynamics across the blood-brain-barrier (BBB) were determined over various time spans ($t_0 = 0$ minutes, before anti-Aβ antibody [α-Aβ] injection, baseline plasma Aβ levels, $t_{10} = 10$ minutes after α-Aβ injection and t_{40}). $^{T}P < .1$, $^{*}P < .05$, $^{**}P < .01$, $^{***}P < .001$ (Student *t* test and Bonferroni correction for comparison of two groups, 2-way ANOVA and Bonferroni *post hoc* test for multiple groups' comparison). $n = 8$ per genotype and treatment. Results are shown as mean ± SEM.

in transgenics but in wildtypes presumably due to the general increase of vessel density. Cerebral LRP1 and MDR1 protein levels increased (the first one in transgenics by trend) after anti-KLK8 antibody delivery (Fig. 4M and 4N), suggesting facilitated elimination of cerebral Aβ via BBB-mediated clearance. To directly test this hypothesis, we determined the kinetics of Aβ efflux from the brain to blood in transgenics, using a modified protocol from Castellano et al. [27]. 10 and 40 min (=t_{10} and t_{40}) after intravenous injection of an Aβ stabilizing anti-Aβ antibody (HJ5.1, enters brain parenchyma only marginally, does not affect the Aβ-brain-to-blood-equilibrium, and protects Aβ from enzymatic digestion), blood plasma $Aβ_{40}$ and $Aβ_{42}$ levels were determined. Anti-KLK8 antibody treatment increased plasma $Aβ_{40}$ at t_{10} (and at t_{40} by trend) as well as $Aβ_{42}$ at t_{40}, indicating improved Aβ clearance across the BBB (Fig. 4O).

3.7. *KLK8 blockade induces autophagy and Aβ phagocytosis*

Autophagy-controlled intracellular clearance of organelles, proteins, and peptides is impaired in the brains of AD patients [13] and transgenic mice [14]. EPHB2 induction appears to promote autophagy under neoplastic conditions [7,8]. We therefore asked whether KLK8 inhibition and the resulting EPHB2 protection are able to counteract autophagy deficits in the AD-affected brain. First, we corroborated an AD-related cerebral perturbation of autophagy modulators, that is, beclin-1, involved in the initiation of autophagosome assemblies [30], and STX17, a protein that triggers fusion of autophagosomes with lysosomes [31] in both mouse (Supplementary Fig. 3A and 3B) and man (Supplementary Fig. 3C and 3D).

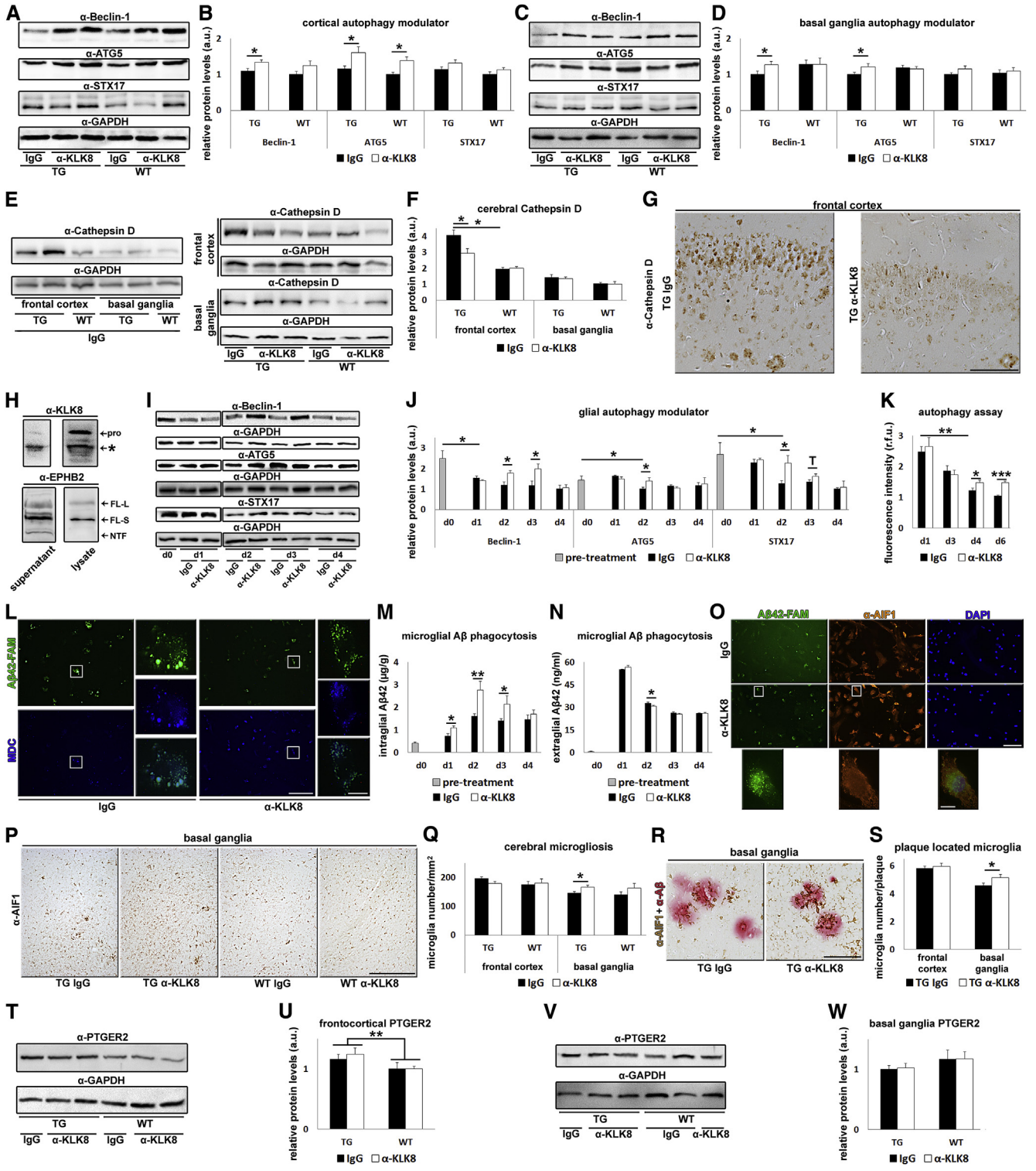

Fig. 5. KLK8 inhibition boosts the autophagy machinery and microglial Aβ phagocytosis in murine brain and *in vitro*. Levels of beclin-1, ATG5 and STX17 in IgG, and anti-KLK8 antibody-treated (α-KLK8) transgenic (TG) and wildtype (WT) mice in the frontal cortex (A, B) and basal ganglia (C, D). (E, F) Cathepsin D levels in the frontal cortex and basal ganglia of TG and WT mice after IgG or α-KLK8 treatment. (G) Representative anti-cathepsin D immunostaining of the frontal cortex in TG mice treated with IgG (left image) or α-KLK8 (right image) demonstrate reduced cathepsin D accumulation after KLK8 blockade. Scale bar: 100 μm. (H) Primary glia were plated (astrocytes:microglia = 1:1) at DIV15. At DIV17 (before treatment, d0), expression and secretion of KLK8 (upper images) and EPHB2 in its long (FL-L), short (FL-S) splice variants and in secreted form EPHB2-NTF (lower images) were determined in lysates and supernatant. From d0 until d5, glia cells were either incubated with α-KLK8 or with IgG. $A\beta_{42}$ was added to the supernatant at d1. 8h later, as well as between d2 and d6, lysates and supernatant were collected. (I, J) Intraglial beclin-1, ATG5, and STX17 levels between d0 and d4. (K) Fluorescence emission after glial treatment with monodansylcadaverine (MDC, a probe detecting autophagic vacuoles) between d1 and d6. (L) After incubation with $A\beta_{42}$-FAM and MDC, α-KLK8-

The next step was to assess the protein levels of beclin-1, ATG5 (essential for the autophagosome assembly [32]) and STX17 in anti-KLK8 antibody versus IgG-treated mice. In transgenics (and to a lesser extend in wildtypes), KLK8 inhibition elevated the levels of beclin-1 and ATG5 in the frontal cortex and basal ganglia (Fig. 5A–5D). By rescuing the autophagy machinery, anti-KLK8 antibody treatment also reversed the cortical accumulation of intraneuronal cathepsin D (Fig. 5E–5G) —a lysosomal enzyme, which (as shown also by others [33,34]) is present in excess in murine and human AD-affected brain. The levels of cathepsin D were lower in the basal ganglia *per se* and remained unaffected by treatment (Fig. 5E and 5F).

Impaired Aβ phagocytosis and dysfunctional beclin-1-associated autophagy in the AD-affected brain is tightly linked to reduced microglial activity [35]. Accordingly, we examined the effect of anti-KLK8 antibody treatment on primary transgenic and wildtype microglial/astroglial co-cultures (for experimental design see Supplementary Fig. 4A) after demonstrating KLK8 secretion and EPHB2 expression (but virtually no Aβ generation) in these naïve cells (Fig. 5H). Although incubation with $A\beta_{42}$ (at d1) knocked down the expression levels of glial autophagy molecules beclin-1, ATG5, and STX17 and weakened fluorescence emission in the autophagy assay, simultaneous co-treatment with anti-KLK8 antibody protected the autophagy machinery in both transgenic and wildtype glial cells (Fig. 5I–5L). Of note, anti-KLK8 antibody treatment doubled intramicroglial $A\beta_{42}$ levels (co-localizing with microglial marker AIF1, Fig. 5M and 5O), whereas $A\beta_{42}$ levels in the supernatant were reduced when compared to IgG control (Fig. 5N and 5O), pinpointing an enhanced clearance of extracellular $A\beta_{42}$ via microglial phagocytosis.

To test whether the positive effects of KLK8 inhibition on autophagy protection and Aβ clearance were transduced by EPHB2 receptor, we co-incubated anti-KLK8 antibody-treated glial cells with an EPHB2 inhibitory antibody (previously used in [3]). In spite of anti-KLK8-antibody presence, inhibition of EPHB2 abolished autophagy and reduced microglial Aβ clearance to levels indistinguishable from or even, below IgG control treated cells, underlining the decisive role of EPHB2 in this context (Supplementary Fig. 4B–4G). Prolonged cell viability monitoring for up to 11 days of treatment revealed that neither anti-KLK8 antibody nor anti-EPHB2 antibody affected glial survival or proliferation (Supplementary Fig. 4H). A genotype-specific difference in basal autophagy and Aβ phagocytosis efficacy could not be detected in primary glia (data not shown), supporting the data of previous publications that microglial functional impairment coincides with amyloid deposition and does not precede it [36].

Next, we searched for evidence of an enhanced microglial Aβ phagocytosis triggered by KLK8 inhibition *in vivo*. Stereological quantification revealed an increase in the total number of activated AIF1-positive microglia in the basal ganglia (but not frontal cortex) of transgenic (but not wildtype) mice (Fig. 5P and 5Q). Additionally, the average number of microglia per plaque was elevated in the basal ganglia (but not in frontal cortex) in verum-treated transgenics (Fig. 5R and 5S). As the expression of the pro-inflammatory prostaglandin E receptor 2 (PTGER2) was not affected by anti-KLK8 antibody treatment (Fig. 5T–5W), the utilization of anti-KLK8 antibody seems to promote the proliferation of phagocytic rather than cytotoxic microglia, plaque approximation, and subsequent Aβ uptake also *in vivo*. Together, our *in vitro* and *in vivo* data strongly support that KLK8 inhibition induces autophagy and Aβ clearance via microglial phagocytosis.

3.8. KLK8 blockade counteracts tau pathology

Although TgCRND8 mice are not a model of primary tau pathology, they display abnormal tau processing as a consequence of Aβ pathology [37]. As it has been recently shown that ligand-triggered stimulation of EPHB2 attenuates tau hyperphosphorylation in tau-transgenic mice [19], we next examined whether KLK8 inhibition and subsequent EPHB2 restoration might reverse Aβ-related tau hyperphosphorylation in TgCRND8 mice as well. We found that 4 weeks of anti-KLK8 antibody administration reduced the ratio of neuritic plaques (containing phospho-tau positive dystrophic neurites) in relationship to total number of Aβ plaques (Fig. 6A and 6B) and lessened tau phosphorylation at amino acids S202/T205, S396, and T212/S214 (Fig. 6C and 6D). The neuroprotective effect of anti-KLK8 therapy against tau hyperphosphorylation was mediated by

treated glia (five images on the right) demonstrate increased MDC incorporation, indicating increased autophagic vacuole density when compared to IgG-treated glia (five images on the left) at d6. Scale bar: 100 μm. Microglia depicted in the smaller images demonstrate swollen autophagic vacuoles heavily loaded with $A\beta_{42}$-FAM in the IgG group and smaller autophagic vacuoles in α-KLK8-treated glia. Scale bar: 10 μm. Intraglial (M) and extraglial (N) $A\beta_{42}$ levels between d0 and d4. (O) Fluorescence images of IgG (upper row) and α-KLK8-treated (lower row) glia incubated with $A\beta_{42}$-FAM and α-AIF1 at d2, demonstrating increased AIF1 signal and hence microglial activation, increased intra-microglial $A\beta_{42}$-FAM, and reduced extra-glial $A\beta_{42}$-FAM signal in α-KLK8-treated glia, indicating enhanced Aβ phagocytosis. Scale bars: 100 μm (upper image) and 10 μm (lower image). (P) Anti-AIF1 immunostaining of basal ganglia of IgG or α-KLK8-treated TG and WT mice. Scale bar: 500 μm. (Q) Stereological quantification of microglial density in the frontal cortex and basal ganglia. (R) Anti-AIF1 and anti-Aβ double immunostaining of basal ganglia of IgG or α-KLK8-treated TG mice. Scale bar: 100 μm. (S) Number of microglia surrounding Aβ plaques in the frontal cortex and basal ganglia. Cerebral expression of the pro-inflammatory PTGER2 remained unchanged after α-KLK8 treatment ([T, U] in the frontal cortices; [V, W] in the basal ganglia), with PTGER2 levels being increased in frontal cortices of diseased mice. $^{T}P < .1$, $^{*}P < .05$, $^{**}P < .01$, $^{***}P < .001$ (2-way ANOVA and Bonferroni *post hoc* test). $n = 8$ per murine group. $n = 6$–8 cell culture plates from three independent batches per treatment condition and test day. Data represent the mean ± s.e.m.

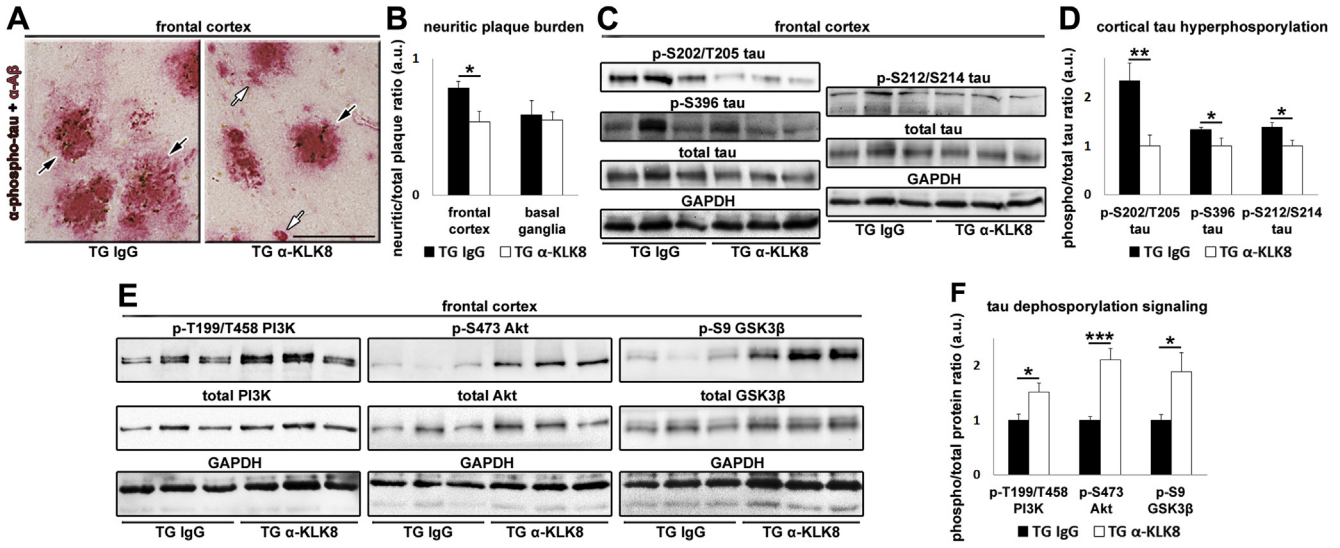

Fig. 6. Anti-KLK8 antibody treatment counteracts tau pathology. (A) Anti-phospho-tau (AT8) and anti-Aβ double immunostaining showing neuritic, AT8-positive (black arrows) and non-neuritic, AT8-negative (white arrows) Aβ plaques in the frontal cortex of transgenic (TG) mice treated with IgG or anti-KLK8 antibody (α-KLK8). Scale bar: 100 μm. (B) Stereological quantification of the neuritic to total plaque ratio in the frontal cortex and basal ganglia. (C, D) Levels of tau phosphorylation at S202/T205, S396, and T212/S214 normalized against total tau amounts and GAPDH. (E, F) Levels of PI3K phosphorylation at T199/T458, Akt phosphorylation at S473 and GSK3β phosphorylation at S9, normalized against levels of total PI3K, Akt or GSK3β, and GAPDH. $^{*}P < .05$, $^{**}P < .01$, $^{***}P < .001$ (Student *t* test and Bonferroni correction for multiple testing). $n = 8$ per treatment. Results are shown as mean ± SEM.

activation of PI3K (indicated by increased phosphorylation of PI3K at T199/T458) as well as Akt (indicated by increased phosphorylation of Akt at S473) and thus downstream inhibition of GSK3β (indicated by increased phosphorylation of GSK3β at S9; Fig. 6E and 6F).

4. Discussion

In line with the limited prior research in this area [15–17], we demonstrate here an AD-related KLK8 excess and EPHB2 deficit in both murine and human hippocampi. We now expand these findings to show a sustained surplus of KLK8 mRNA and protein in different brain regions, both in AD-affected and rarely affected brain areas such as the entorhinal cortex and cerebellum, respectively. Besides considerable similarities in the (pathologic) expression patterns of KLK8 and its downstream signaling molecules EPHB2/FKBP5/EFNB2 in mouse and man, there were also some interspecies discrepancies which are explicable through species differences *per se*, differences in the disease genetic background (early onset familiar AD mouse model with $hAPP_{Swedish/Indiana}$ mutations vs. late-onset sporadic AD patients) and most importantly age and disease stage differences (with mice being examined at P30/P90/P210/P360 which equate to childhood/adolescence/middle-aged and/or old aged and humans at on average 75 years of age in the AD and old control groups and 31 years in young control group). Of note, the interspecies match was highest for KLK8 followed by its proteolytic substrate EPHB2 and the downstream signaling molecule FKPB5, and lowest for EFNB2. Irrespective of these differences, KLK8 excess occurs in both species very early in the course of the disease and before the depletion of its proteolytic target EPHB2, that is, in mice before Aβ pathology onset and in humans in preclinical stages.

This exceedingly early and multifocal event is suggestive of a key and causative role for KLK8 in the pathogenesis of AD. To our knowledge, our study is the first to provide evidence that the inhibition of KLK8 attenuates multiple primary and secondary dysfunctions evolving during the course of AD. We show that KLK8 blockade in TgCRND8 mice diminishes amyloidogenic APP processing, improves neurovascular function and Aβ clearance across the BBB, enhances microglial Aβ phagocytosis and autophagy, and thereby reduces cerebral Aβ load. It further suppresses tau phosphorylation signaling and reverses abnormal tau phosphorylation. In addition to targeting Aβ and tau metabolism, down-regulation of KLK8 activity normalizes the molecular signatures of anxiety in the amygdala and induces structural neuroplasticity in the hippocampus, resulting in less fearful behavior and better memory performance in transgenic mice.

Further work should investigate which of the molecular, structural, and behavioral improvements are immediate consequences of KLK8 blockade, secondary effects of EPHB2 protection, or tertiary signs of integral amelioration. For example, the effects on the autophagy machinery and microglial Aβ clearance appear to be directly attributable to anti-KLK8 treatment and EPHB2 dependent. Treatment-induced anxiolytic effects are probably also the immediate consequence of reduced KLK8 activity and diminished EPHB2 fragmentation, resulting in FKBP5 and glucocorticoid receptor suppression, a mechanism first described by Attwood

et al. [3]. Attenuated tau pathology, however, is likely to be in part a direct consequence of anti-KLK8-triggered suppression of tau phosphorylation signals but also an indirect result of Aβ decline and reduced neurotoxicity. Likewise, the effects of anti-KLK8 treatment on Aβ generation/Aβ aggregation/neurovascular dysfunction could arise from immediate affecting of only one member of this loop and subsequently indirect influencing of the other components by breaking the ongoing "vicious circle". If this is the case, the question remains as to which component is the initial target.

Furthermore, EPHB2-dependent and EPHB2-independent effects of KLK8 blockade should be distinguished, in particular because KLK8 has additional substrates besides EPHB2 with possible AD implications. Our BLAST analysis of the KLK8 target recognition sequence YGRY [3] identified eight-putative and one-assured [2] KLK8 substrates. Two of these proteins, that is, fibronectin and steroid 5 alpha-reductase 1 (Srd5a1), play a role in AD and are therefore candidates for further testing in the context of anti-KLK8 therapy. Cerebral fibronectin levels are reduced already before AD onset in patients with mild cognitive impairment [38]. Moreover, fibronectin promotes the secretion of APP and impedes APP integration into plasma membranes and subsequent Aβ biogenesis [39]. Accordingly, putative enhancement of fibronectin due to KLK8 inhibition would offer an explanation of how anti-KLK8 treatment inhibits amyloidogenic APP processing and Aβ generation. This explanation is of particular interest because, based on KLK8 target recognition sequence [3], neither APP processing secretases nor APP itself interacts directly with KLK8. The other potential KLK8 substrate candidate, Srd5a1 participates in the biosynthesis of allopregnanolone which is a neurosteroid with anxiolytic properties [40]. AD patients have reduced allopregnanolone levels [41], whereas allopregnanolone administration improves cognitive performance and promotes hippocampal neurogenesis in the 3xTg AD mouse model [42,43]. Further investigations should verify the effects of anti-KLK8 treatment on fibronectin as well as Srd5a1-mediated allopregnanolone biosynthesis.

To exploit the therapeutic potential of anti-KLK8 treatment, optimal antibody dose and treatment period must be established. Our results indicate that KLK8 inhibition interferes with early steps of the amyloid cascade, suggesting possible prophylactic properties in the early disease stages. Conversely, 4 weeks of antibody application was sufficient to exert therapeutic effects in mice with moderate AD pathology, hinting at potential curative benefits also in later disease stages. Moreover, KLK8 should be evaluated as an antecedent plasma and/or cerebrospinal fluid (CSF) biomarker, as its cerebral expression is already increased in preclinical stages of AD.

Ultimately, the most intriguing issue remains to verify the bench-to-bedside translational potential of this novel therapeutic approach.

Acknowledgments

Parts of this study were supported by a grant from German Research Foundation (DFG, Grant HE 6823/3-1 and KE 1134/7-1) and Internal Research Funding Essen (IFORES) of the University Duisburg-Essen (Grant D/107-81030). We thank Michaela Knoll, Nicole Macha, and Dr. Norbert Buresch for excellent technical assistance.

Supplementary data

Supplementary data related to this article can be found at http://dx.doi.org/10.1016/j.jalz.2016.05.006.

RESEARCH IN CONTEXT

1. Systematic review: The clinical hallmarks of Alzheimer's disease (AD) are memory loss and increased anxiety. We hypothesized that the protease kallikrein-8 (KLK8) is involved in the pathogenesis of AD, as it is implicated in memory acquisition and anxiety and its mRNA is elevated in AD-affected human hippocampus.
2. Interpretation: The present study identifies KLK8 as a possible antecedent biomarker of AD, as it was drastically increased in both murine and human brain before disease onset and qualifies this molecule as a potential therapeutic target against AD, as antibody-mediated KLK8 inhibition in an early disease stage attenuated multiple AD-related behavioral, structural, and molecular impairments in TgCRND8 mice.
3. Future directions: Future investigations should determine the optimal dose and treatment window for the anti-KLK8 therapy, evaluate KLK8 as a CSF and/or plasma biomarker and validate the bench-to-bedside translational potential of anti-KLK8 therapy in AD patients.

References

[1] Tamura H, Kawata M, Hamaguchi S, Ishikawa Y, Shiosaka S. Processing of neuregulin-1 by neuropsin regulates GABAergic neuron to control neural plasticity of the mouse hippocampus. J Neurosci 2012; 32:12657–72.
[2] Shimizu C, Yoshida S, Shibata M, Kato K, Momota Y, Matsumoto K, et al. Characterization of recombinant and brain neuropsin, a plasticity-related serine protease. J Biol Chem 1998;273:11189–96.
[3] Attwood BK, Bourgognon JM, Patel S, Mucha M, Schiavon E, Skrzypiec AE, et al. Neuropsin cleaves EphB2 in the amygdala to control anxiety. Nature 2011;473:372–5.
[4] Srivastava N, Robichaux MA, Chenaux G, Henkemeyer M, Cowan CW. EphB2 receptor forward signaling controls cortical

growth cone collapse via Nck and Pak. Mol Cell Neurosci 2013; 52:106–16.
[5] Kayser MS, Nolt MJ, Dalva MB. EphB receptors couple dendritic filopodia motility to synapse formation. Neuron 2008;59:56–69.
[6] Adams RH, Wilkinson GA, Weiss C, Diella F, Gale NW, Deutsch U, et al. Roles of ephrinB ligands and EphB receptors in cardiovascular development: demarcation of arterial/venous domains, vascular morphogenesis, and sprouting angiogenesis. Genes Dev 1999;13:295–306.
[7] Chukkapalli S, Amessou M, Dilly AK, Dekhil H, Zhao J, Liu Q, et al. Role of the EphB2 receptor in autophagy, apoptosis and invasion in human breast cancer cells. Exp Cell Res 2014;320:233–46.
[8] Kandouz M, Haidara K, Zhao J, Brisson ML, Batist G. The EphB2 tumor suppressor induces autophagic cell death via concomitant activation of the ERK1/2 and PI3K pathways. Cell Cycle 2010;9:398–407.
[9] D'Amelio M, Rossini PM. Brain excitability and connectivity of neuronal assemblies in Alzheimer's disease: from animal models to human findings. Prog Neurobiol 2012;99:42–60.
[10] Ruan L, Lau BW, Wang J, Huang L, Zhuge Q, Wang B, et al. Neurogenesis in neurological and psychiatric diseases and brain injury: from bench to bedside. Prog Neurobiol 2014;115:116–37.
[11] Zlokovic BV. Neurovascular pathways to neurodegeneration in Alzheimer's disease and other disorders. Nat Rev Neurosci 2011; 12:723–38.
[12] Paris D, Ganey N, Banasiak M, Laporte V, Patel N, Mullan M, et al. Impaired orthotopic glioma growth and vascularization in transgenic mouse models of Alzheimer's disease. J Neurosci 2010;30:11251–8.
[13] Ghavami S, Shojaei S, Yeganeh B, Ande SR, Jangamreddy JR, Mehrpour M, et al. Autophagy and apoptosis dysfunction in neurodegenerative disorders. Prog Neurobiol 2014;112:24–49.
[14] Yang DS, Stavrides P, Mohan PS, Kaushik S, Kumar A, Ohno M, et al. Reversal of autophagy dysfunction in the TgCRND8 mouse model of Alzheimer's disease ameliorates amyloid pathologies and memory deficits. Brain 2011;134:258–77.
[15] Shimizu-Okabe C, Yousef GM, Diamandis EP, Yoshida S, Shiosaka S, Fahnestock M. Expression of the kallikrein gene family in normal and Alzheimer's disease brain. Neuroreport 2001;12:2747–51.
[16] Qu M, Jiang J, Liu XP, Tian Q, Chen LM, Yin G, et al. Reduction and the intracellular translocation of EphB2 in Tg2576 mice and the effects of beta-amyloid. Neuropathol Appl Neurobiol 2013;39:612–22.
[17] Simon AM, de Maturana RL, Ricobaraza A, Escribano L, Schiapparelli L, Cuadrado-Tejedor M, et al. Early changes in hippocampal Eph receptors precede the onset of memory decline in mouse models of Alzheimer's disease. J Alzheimers Dis 2009;17:773–86.
[18] Cisse M, Halabisky B, Harris J, Devidze N, Dubal DB, Sun B, et al. Reversing EphB2 depletion rescues cognitive functions in Alzheimer model. Nature 2011;469:47–52.
[19] Jiang J, Wang ZH, Qu M, Gao D, Liu XP, Zhu LQ, et al. Stimulation of EphB2 attenuates tau phosphorylation through PI3K/Akt-mediated inactivation of glycogen synthase kinase-3beta. Sci Rep 2015;5:11765.
[20] Chishti MA, Yang DS, Janus C, Phinney AL, Horne P, Pearson J, et al. Early-onset amyloid deposition and cognitive deficits in transgenic mice expressing a double mutant form of amyloid precursor protein 695. J Biol Chem 2001;276:21562–70.
[21] Mirra SS, Hart MN, Terry RD. Making the diagnosis of Alzheimer's disease. A primer for practicing pathologists. Arch Pathol Lab Med 1993;117:132–44.
[22] Braak H, Braak E. Neuropathological stageing of Alzheimer-related changes. Acta Neuropathol 1991;82:239–59.
[23] Momota Y, Yoshida S, Ito J, Shibata M, Kato K, Sakurai K, et al. Blockade of neuropsin, a serine protease, ameliorates kindling epilepsy. Eur J Neurosci 1998;10:760–4.
[24] Young EJ, Lipina T, Tam E, Mandel A, Clapcote SJ, Bechard AR, et al. Reduced fear and aggression and altered serotonin metabolism in Gtf2ird1-targeted mice. Genes Brain Behav 2008;7:224–34.
[25] Kilic E, ElAli A, Kilic U, Guo Z, Ugur M, Uslu U, et al. Role of Nogo-A in neuronal survival in the reperfused ischemic brain. J Cereb Blood Flow Metab 2010;30:969–84.
[26] Sunyer B, Patil S, Höger H, Lubec G. Barnes maze, a useful task to assess spatial reference memory in the mice. Protoc Exchange 2007. Available at: http://www.nature.com/protocolexchange/protocols/349. Accessed June 19, 2016.
[27] Castellano JM, Deane R, Gottesdiener AJ, Verghese PB, Stewart FR, West T, et al. Low-density lipoprotein receptor overexpression enhances the rate of brain-to-blood Abeta clearance in a mouse model of beta-amyloidosis. Proc Natl Acad Sci U S A 2012; 109:15502–7.
[28] Herring A, Donath A, Yarmolenko M, Uslar E, Conzen C, Kanakis D, et al. Exercise during pregnancy mitigates Alzheimer-like pathology in mouse offspring. FASEB J 2012;26:117–28.
[29] Tamura H, Ishikawa Y, Hino N, Maeda M, Yoshida S, Kaku S, et al. Neuropsin is essential for early processes of memory acquisition and Schaffer collateral long-term potentiation in adult mouse hippocampus in vivo. J Physiol 2006;570:541–51.
[30] Fimia GM, Di Bartolomeo S, Piacentini M, Cecconi F. Unleashing the Ambra1-Beclin 1 complex from dynein chains: Ulk1 sets Ambra1 free to induce autophagy. Autophagy 2011;7:115–7.
[31] Itakura E, Kishi-Itakura C, Mizushima N. The hairpin-type tail-anchored SNARE syntaxin 17 targets to autophagosomes for fusion with endosomes/lysosomes. Cell 2012;151:1256–69.
[32] Pyo JO, Yoo SM, Ahn HH, Nah J, Hong SH, Kam TI, et al. Overexpression of Atg5 in mice activates autophagy and extends lifespan. Nat Commun 2013;4:2300.
[33] Wirths O, Breyhan H, Marcello A, Cotel MC, Bruck W, Bayer TA. Inflammatory changes are tightly associated with neurodegeneration in the brain and spinal cord of the APP/PS1KI mouse model of Alzheimer's disease. Neurobiol Aging 2010;31:747–57.
[34] Cataldo AM, Barnett JL, Berman SA, Li J, Quarless S, Bursztajn S, et al. Gene expression and cellular content of cathepsin D in Alzheimer's disease brain: evidence for early up-regulation of the endosomal-lysosomal system. Neuron 1995;14:671–80.
[35] Lucin KM, O'Brien CE, Bieri G, Czirr E, Mosher KI, Abbey RJ, et al. Microglial beclin 1 regulates retromer trafficking and phagocytosis and is impaired in Alzheimer's disease. Neuron 2013;79:873–86.
[36] Krabbe G, Halle A, Matyash V, Rinnenthal JL, Eom GD, Bernhardt U, et al. Functional impairment of microglia coincides with Beta-amyloid deposition in mice with Alzheimer-like pathology. PLoS One 2013; 8:e60921.
[37] Bellucci A, Rosi MC, Grossi C, Fiorentini A, Luccarini I, Casamenti F. Abnormal processing of tau in the brain of aged TgCRND8 mice. Neurobiol Dis 2007;27:328–38.
[38] Muenchhoff J, Poljak A, Song F, Raftery M, Brodaty H, Duncan M, et al. Plasma protein profiling of mild cognitive impairment and Alzheimer's disease across two independent cohorts. J Alzheimers Dis 2015;43:1355–73.
[39] Monning U, Sandbrink R, Weidemann A, Banati RB, Masters CL, Beyreuther K. Extracellular matrix influences the biogenesis of amyloid precursor protein in microglial cells. J Biol Chem 1995; 270:7104–10.
[40] Guidotti A, Costa E. Can the antidysphoric and anxiolytic profiles of selective serotonin reuptake inhibitors be related to their ability to increase brain 3 alpha, 5 alpha-tetrahydroprogesterone (allopregnanolone) availability? Biol Psychiatry 1998;44:865–73.
[41] Naylor JC, Kilts JD, Hulette CM, Steffens DC, Blazer DG, Ervin JF, et al. Allopregnanolone levels are reduced in temporal cortex in patients with Alzheimer's disease compared to cognitively intact control subjects. Biochim Biophys Acta 2010;1801:951–9.
[42] Wang JM, Singh C, Liu L, Irwin RW, Chen S, Chung EJ, et al. Allopregnanolone reverses neurogenic and cognitive deficits in mouse model of Alzheimer's disease. Proc Natl Acad Sci U S A 2010; 107:6498–503.
[43] Chen S, Wang JM, Irwin RW, Yao J, Liu L, Brinton RD. Allopregnanolone promotes regeneration and reduces beta-amyloid burden in a preclinical model of Alzheimer's disease. PLoS One 2011; 6:e24293.